Calculation of thermal-diffusion coefficients from plane-wave fluctuations in the heat energy density

Bruce J. Palmer
Analytic Sciences Department, Pacific Northwest Laboratory, Richland, Washington 99352
(Received 4 October 1993)

A method to calculate the thermal diffusivity D_T from spontaneous fluctuations in the local heat energy density is presented. Calculations of the thermal diffusivity are performed for the Lennard-Jones fluid, carbon dioxide, and water. The results for the Lennard-Jones fluid are in agreement with calculations of the thermal conductivity using Green-Kubo relations and nonequilibrium molecular-dynamics techniques. The results for carbon dioxide and water give thermal diffusivities within a factor of 2 of the experimental values.

PACS number(s): 05.60.+w, 02.70.Ns, 66.60.+a

I. INTRODUCTION

This paper will explore the calculation of the thermal diffusivity from molecular-dynamics simulations based on the decay of spontaneous fluctuations in the heat energy density. This is similar to an approach for calculating the shear viscosity based on the decay of spontaneous fluctuations in the transverse velocity fields [1–3]. Previous studies of heat transfer in molecular simulations have focused on the thermal conductivity κ which is closely related to the thermal diffusivity D_T via the equation [4]

$$D_T=\rho c_p \kappa \ , \tag{1.1}$$

where ρ is the density and c_p is the constant-pressure specific heat. Most calculations of the thermal conductivity have used either nonequilibrium molecular-dynamics (NEMD) techniques [5–7] or the appropriate Green-Kubo relations [8–10]. For the NEMD calculation, the response of the system to a small disturbance is calculated and compared to the same system in the absence of the disturbance. The Green-Kubo relation requires the evaluation of a time correlation function formed from components of the energy current. The thermal conductivity can then be calculated by integrating over the time correlation function.

Both the NEMD techniques and the Green-Kubo relation appear to work well. The thermal conductivity can be calculated with small uncertainties (typically less than 5%) with reasonable effort, and both methods agree with each other in cases where they can be compared directly [5–8]. However, the use of NEMD techniques limits the amount of additional information that can be gained from the simulation, and the calculation of the Green-Kubo integrand during an equilibrium simulation adds substantially to the force loop calculation [11].

An alternative to these methods is to monitor the decay of spontaneous fluctuations in the heat energy density. This is analogous to an approach for calculating the shear viscosity by examining the long-time behavior of the transverse current autocorrelation function (TCAF) [1–3]. Correlation functions can be formed from plane-wave expansions of the local heat energy density. Those correlation functions that are formed from the long-wavelength components of the expansion decay exponentially at long times, with a decay constant that is proportional to the thermal-diffusion coefficient. For large systems, the correlation functions can be calculated easily during the simulation and the thermal diffusivity can be recovered from the long-time behavior. This procedure is easily implemented and does not add significantly to the computational requirements for the simulation. It gives results that are in agreement with other methods, although the overall statistics do not appear quite as good.

II. BACKGROUND

A brief derivation of the equations governing thermal diffusion is given in this section. This derivation is intended to give a qualitative sketch of the relation between the microscopic behavior of the liquid and the macroscopic thermal-diffusion coefficient. More rigorous derivations based on linear-response theory can be found in the literature [12–14].

The treatment of thermal diffusion in a liquid begins with the conservation law

$$\frac{\partial}{\partial t}\epsilon(\mathbf{r},t)+\nabla\cdot\mathbf{j}^{\epsilon}(\mathbf{r},t)=0 \ , \tag{2.1}$$

where $\epsilon(\mathbf{r},t)$ is the spatially dependent energy density and $\mathbf{j}^{\epsilon}(\mathbf{r},t)$ is the corresponding energy current. For a system moving with constant uniform velocity $\mathbf{v}$, the energy current $\mathbf{j}^{\epsilon}$ has the form

$$\mathbf{j}^{\epsilon}=(\epsilon+p)\mathbf{v} \ . \tag{2.2}$$

The hydrostatic pressure p appearing in Eq. (2.2) accounts for the pdV work that is done when the flow is no longer uniform.

For a nonuniform system with temperature gradients, the energy current is modified to

$$\mathbf{j}^{\epsilon}(\mathbf{r},t)=(\epsilon+p)\mathbf{v}(\mathbf{r},t)-\kappa\nabla T(\mathbf{r},t) \ , \tag{2.3}$$

where $T(\mathbf{r},t)$ is the local temperature and κ is the thermal conductivity. The final term accounts for the energy currents that appear when a thermal gradient exists.

All spatially dependent quantities are assumed to be small. Inserting this expression for $\mathbf{j}^{\epsilon}$ into the conservation law (2.1) gives

$$\frac{\partial}{\partial t}\epsilon(\mathbf{r},t)+(\epsilon+p)\nabla\cdot\mathbf{v}(\mathbf{r},t)-\kappa\nabla^2 T(\mathbf{r},t)=0 \ . \tag{2.4}$$

The $\nabla\cdot\mathbf{v}(\mathbf{r},t)$ term in Eq. (2.4) can be eliminated using the mass conservation equation

$$\frac{\partial\rho}{\partial t}+\nabla\cdot(\rho\mathbf{v})=0 \ , \tag{2.5}$$

where $\rho(\mathbf{r},t)$ is the local mass density. Substituting Eq. (2.5) in Eq. (2.4) and retaining only the terms that are linear in small quantities gives [12]

$$\frac{\partial}{\partial t}\left[\epsilon(\mathbf{r},t)-\frac{\epsilon+p}{\rho}\rho(\mathbf{r},t)\right]-\kappa\nabla^2 T(\mathbf{r},t)=0 \ . \tag{2.6}$$

The quantity in brackets is referred to as the heat energy density

$$q(\mathbf{r},t)=\epsilon(\mathbf{r},t)-\frac{\epsilon+p}{\rho}\rho(\mathbf{r},t) \ . \tag{2.7}$$

To solve Eq. (2.6), the Fourier and Laplace transform of $q(\mathbf{r},t)$ is defined as

$$q(\mathbf{k},z)=\int dr^3 e^{i\mathbf{k}\cdot\mathbf{r}}\int_0^\infty dt\, e^{izt}q(\mathbf{r},t) \ . \tag{2.8}$$

A similar expression exists for $T(\mathbf{r},t)$. The Fourier-Laplace transform of Eq. (2.6) is the algebraic equation

$$-iz\,q(\mathbf{k},z)+\kappa k^2 T(\mathbf{k},z)=q(\mathbf{k}) \ , \tag{2.9}$$

where $q(\mathbf{k})$ is the Fourier transform of $q(\mathbf{r},t=0)$.

The next step is to rewrite $T(\mathbf{k},z)$ in terms of $q(\mathbf{k},z)$. This can be done by using the thermodynamic identity

$$TdS=dE+pdV \ , \tag{2.10}$$

where E and S are the energy and entropy of the system, respectively. If the total number of molecules in the system is fixed, implying that the total mass is fixed, then fluctuations in ρ and V are related via

$$-\frac{dV}{V}=\frac{d\rho}{\rho} \ . \tag{2.11}$$

This leads to

$$\begin{aligned} dE&=d(\epsilon V)=Vd\epsilon+\epsilon dV \\ &=V\left[d\epsilon-\frac{\epsilon}{\rho}d\rho\right] \ . \end{aligned}$$

Thus, for a constant number of molecules,

$$\frac{T}{V}dS=d\epsilon-\frac{\epsilon+p}{\rho}d\rho \ . \tag{2.12}$$

From Eq. (2.12), q can be interpreted as a local entropy density and fluctuations in q under constant-pressure conditions can be equated with fluctuations in the local enthalpy. Instead of using q and T as variables, it is more convenient to use q and p. Expanding $T(\mathbf{k},z)$ in terms of $q(\mathbf{k},z)$ and $p(\mathbf{k},z)$ gives

$$T(\mathbf{k},z)=\left.\frac{\partial T}{\partial p}\right|_S p(\mathbf{k},z)+\frac{V}{T}\left.\frac{\partial T}{\partial S}\right|_p q(\mathbf{k},z) \ . \tag{2.13}$$

Equation (2.13) follows directly from Eq. (2.12). The derivative of temperature with respect to entropy is related to the constant-pressure specific heat via

$$\rho c_p=\frac{T}{V}\left.\frac{\partial S}{\partial T}\right|_p \ . \tag{2.14}$$

Equation (2.9) can then be written as

$$-izq(\mathbf{k},z)+\rho c_p\kappa k^2 q(\mathbf{k},z)=q(\mathbf{k})-\kappa k^2\left.\frac{\partial T}{\partial p}\right|_S p(\mathbf{k},z) \ , \tag{2.15}$$

which can be solved for $q(\mathbf{k},z)$ to give [15]

$$\begin{aligned} q(\mathbf{k},z)=&\frac{1}{-iz+D_T k^2}q(\mathbf{k}) \\ &-\frac{k^2}{-iz+D_T k^2}\kappa\left.\frac{\partial T}{\partial p}\right|_S p(\mathbf{k},z) \ . \end{aligned} \tag{2.16}$$

At long wavelengths (small k), the second term in Eq. (2.16) can be ignored. The correlation function for spontaneous fluctuations in q should then have the form

$$\langle q(\mathbf{k},z)q(\mathbf{k})\rangle=\frac{1}{-iz+D_T k^2}\langle(q(\mathbf{k}))^2\rangle \ . \tag{2.17}$$

The brackets represent an equilibrium average over initial conditions. This equation applies only in the hydrodynamic limit of small k and long times. The real-time equivalent of Eq. (2.17) is

$$\begin{aligned} C_{qq}(\mathbf{k},t)&\equiv\langle q(\mathbf{k},t)q(\mathbf{k})\rangle \\ &\sim e^{-k^2 D_T t} \ . \end{aligned} \tag{2.18}$$

Equation (2.18) provides a direct method for calculating the thermal-diffusion coefficient from molecular-dynamics simulations. The fields $q(\mathbf{k},t)$ are calculated during the simulation and used to form the autocorrelation function $C_{qq}(\mathbf{k},t)$. The thermal-diffusion coefficient can then be extracted from the decay constant for $C_{qq}(\mathbf{k},t)$ at long times, provided that k is small enough so that the hydrodynamic form represented by Eq. (2.18) applies.

The microscopic expressions for the fields $q(\mathbf{k},t)$ can be obtained using standard techniques. The microscopic energy density $\epsilon(\mathbf{r},t)$ and the particle density $\rho(\mathbf{r},t)$ for a system containing N particles can be written as

$$\epsilon(\mathbf{r},t)=\sum_{j=1}^{N}\epsilon_j(t)\delta(\mathbf{r}-\mathbf{r}_j(t)) \ , \tag{2.19}$$

$$\rho(\mathbf{r},t)=\sum_{j=1}^{N}\delta(\mathbf{r}-\mathbf{r}_j(t)) \ , \tag{2.20}$$

where $\mathbf{r}_j(t)$ is the location of particle j at time t. For a monotomic fluid with pairwise additive interactions, the single-particle energy ϵ_j is given by

$$\epsilon_j=\frac{p_j^2}{2m_j}+\frac{1}{2}\sum_{l=1}^{N}\phi_{jl}(r_{jl}) , \tag{2.21}$$

where $\phi_{jl}(r_{jl})$ is the interaction between particles j and l, and m_j and $\mathbf{p}_j$ are the mass and momentum, respectively, of particle j. For a periodic system of volume L^3, the δ functions in Eqs. (2.19) and (2.20) can be expanded as

$$\delta(\mathbf{r}-\mathbf{r}_j(t))=\sum_{\mathbf{k}}\frac{e^{i\mathbf{k}\cdot(\mathbf{r}-\mathbf{r}_j(t))}}{(2\pi L)^3} . \tag{2.22}$$

The sum is over all $\mathbf{k}$ of the form

$$\mathbf{k}=\frac{2\pi}{L}(n_1,n_2,n_3) ,$$

where n_1,n_2,n_3 are integers. This paper will follow the crystallographic convention of labeling all equivalent $\mathbf{k}$ vectors by $(|n_1|,|n_2|,|n_3|)$. Substituting the expansion of the delta function (2.22) into Eq. (2.19) gives the expression

$$\epsilon(\mathbf{r},t)=\sum_{\mathbf{k}}\left[\sum_{j=1}^{N}\epsilon_j(t)e^{-i\mathbf{k}\cdot\mathbf{r}_j(t)}\right]\frac{e^{i\mathbf{k}\cdot\mathbf{r}}}{(2\pi L)^3} . \tag{2.23}$$

The Fourier amplitudes for energy fluctuations are then

$$\epsilon(\mathbf{k},t)=\sum_{j=1}^{N}\epsilon_j(t)e^{-i\mathbf{k}\cdot\mathbf{r}_j(t)} . \tag{2.24}$$

Similarly, the Fourier amplitudes for density fluctuations are

$$\rho(\mathbf{k},t)=\sum_{j=1}^{N}e^{-i\mathbf{k}\cdot\mathbf{r}_j(t)} . \tag{2.25}$$

From Eq. (2.7) the correlation function $C_{qq}(\mathbf{k},t)$ can be written as

$$\begin{aligned}C_{qq}(\mathbf{k},t)=&\langle\epsilon(\mathbf{k},t)\epsilon(\mathbf{k})\rangle-\frac{\epsilon+p}{\rho}\langle\epsilon(\mathbf{k},t)\rho(\mathbf{k})\rangle\\&-\frac{\epsilon+p}{\rho}\langle\rho(\mathbf{k},t)\epsilon(\mathbf{k})\rangle\\&-\left[\frac{\epsilon+p}{\rho}\right]^2\langle\rho(\mathbf{k},t)\rho(\mathbf{k})\rangle .\end{aligned} \tag{2.26}$$

Equation (2.26) is the most convenient form for calculating $C_{qq}(\mathbf{k},t)$ from simulations. The energy density ϵ and the pressure p are average quantities that are known only at the end of the simulation. The four correlation functions $\langle\epsilon(\mathbf{k},t)\epsilon(\mathbf{k})\rangle$, etc., can be calculated during the course of the simulation, and $C_{qq}(\mathbf{k},t)$ is constructed at the end, using Eq. (2.26) when accurate values of ϵ and p are available.

Instead of defining the Fourier amplitudes by Eqs. (2.24) and (2.25), equivalent expressions can be defined with sine and cosine functions. The amplitudes for $\epsilon(\mathbf{k},t)$ now have the form

$$\epsilon(\mathbf{k},t)=\sum_{j=1}^{N}\epsilon_j(t)\sin(\mathbf{k}\cdot\mathbf{r}_j(t)) ,$$

or

$$\epsilon(\mathbf{k},t)=\sum_{j=1}^{N}\epsilon_j(t)\cos(\mathbf{k}\cdot\mathbf{r}_j(t)) .$$

Similar expressions exist for $\rho(\mathbf{k},t)$. If the sine and cosine expansions are used, then the correlation functions for $\mathbf{k}$ and $-\mathbf{k}$ are the same, so the total number of correlation functions associated with all $\mathbf{k}$ vectors of equal magnitude remains the same, whether Eqs. (2.24) and (2.25) or the sine and cosine expansions are used.

For an infinite system, the translational and rotational symmetry of an isotropic liquid means that the $C_{qq}(\mathbf{k},t)$ depend only on the magnitude of $\mathbf{k}$. For finite systems with periodic boundary conditions, this is no longer necessarily true. Only those $C_{qq}(\mathbf{k},t)$ calculated from $\mathbf{k}$'s that are related by symmetries of the periodic lattice must be equivalent. For example, the $C_{qq}(\mathbf{k},t)$ calculated from the $\mathbf{k}$ vectors labeled by the indices (2,2,1) and (3,0,0) could differ. For this case there are two sets of indices, corresponding to vectors of the same length that are not related by symmetry operations of the periodic lattice. Furthermore, $C_{qq}(\mathbf{k},t)$ calculated for the same $\mathbf{k}$ vector could differ if calculated from simulations of different system sizes. For the liquids investigated in this paper, the dependence of the $C_{qq}(\mathbf{k},t)$ on the system size appears negligible.

The Fourier transform of $C_{qq}(\mathbf{k},t)$ is also of interest because of its relation to the Green-Kubo formula for the thermal conductivity. The correlation function $C_{qq}(\mathbf{k},t)$ can be considered symmetric in time about the origin $t=0$, and its Fourier transform is defined as

$$C_{qq}(\mathbf{k},\omega)=\int_{-\infty}^{\infty}e^{i\omega t}C_{qq}(\mathbf{k},t)dt .$$

From linear-response theory, the wave-vector- and frequency-dependent susceptibility for disturbances in the field $q(\mathbf{k},t)$ at small k and ω is [12–14]

$$\chi_{qq}(\mathbf{k},\omega)=\frac{\rho c_p T D_T k^2\omega}{\omega^2+(D_T k^2)^2} . \tag{2.27}$$

The susceptibility $\chi_{qq}(\mathbf{k},\omega)$ can be related to the $C_{qq}(\mathbf{k},\omega)$ using the fluctuation-dissipation theorem to get [13]

$$\chi_{qq}(\mathbf{k},\omega)=\omega k_B T C_{qq}(\mathbf{k},t) . \tag{2.28}$$

The Green-Kubo relation follows from taking the limit

$$\begin{aligned}\kappa=&\frac{1}{T}\lim_{\omega\to 0}\lim_{k\to 0}\frac{\omega}{k^2}\chi_{qq}(\mathbf{k},\omega)\\=&k_B\lim_{\omega\to 0}\lim_{k\to 0}\frac{\omega^2}{k^2}C_{qq}(\mathbf{k},\omega) .\end{aligned} \tag{2.29}$$

The Green-Kubo integral is obtained by converting Eq. (2.29) into its corresponding real-space real-time expression. The small-k, small-ω expression for $C_{qq}(\mathbf{k},\omega)$ follows directly from Eqs. (2.27) and (2.28):

$$C_{qq}(\mathbf{k},\omega)=\frac{\rho c_p D_T k^2/k_B}{\omega^2+(D_T k^2)^2} .$$

This is simply the Fourier transform of Eq. (2.18), so the exponential decay of $C_{qq}(\mathbf{k},t)$ at small k and long times

implies the validity of the Green-Kubo relation. If $C_{qq}(\mathbf{k},t)$ does not exhibit such behavior for the smallest $\mathbf{k}$ accessible in the simulation, this may point to finite-size contributions to the Green-Kubo value of κ.

III. MEMORY FUNCTIONS

To actually obtain the thermal diffusivity, the $C_{qq}(\mathbf{k},t)$ obtained from the simulations are fit to an analytic form and the thermal diffusivity is extracted from the parameters in the fit. The simplest approach is to fit the $C_{qq}(\mathbf{k},t)$ to an exponential decay and calculate D_T from the decay constant. However, it is also possible to generalize the equation for $C_{qq}(\mathbf{k},t)$ to account for nonhydrodynamic effects that occur at short times and small length scales (large k).

Equation (2.17) implies that $C_{qq}(\mathbf{k},t)$ satisfies a real-time equation of the form

$$\frac{\partial}{\partial t}C_{qq}(\mathbf{k},t)=-D_T k^2 C_{qq}(\mathbf{k},t) \ . \tag{3.1}$$

The solution of this equation is the exponential decay in Eq. (2.18). Some of the nonhydrodynamic behavior at short times can be accounted for by generalizing Eq. (3.1) to

$$\frac{\partial}{\partial t}C_{qq}(\mathbf{k},t)=-D_T k^2 \int_0^\infty \phi(t-t')C_{qq}(\mathbf{k},t')dt' \ , \tag{3.2}$$

where the memory function $\phi(t)$ satisfies the normalization condition

$$\int_0^\infty \phi(t)dt=1 \ .$$

For $\phi(t)=\delta(t)$, Eq. (3.2) reduces to Eq. (3.1). A common choice for $\phi(t)$ is a simple exponential relaxation [13],

$$\phi(t)=\frac{1}{\tau}e^{-t/\tau} \ , \tag{3.3}$$

where τ is a microscopic relaxation time. The memory function accounts for the lag between the time a gradient appears in the density $q(\mathbf{r})$ and the appearance of the corresponding current $\mathbf{j}_q$.

For water, a damped oscillation of the form

$$\phi(t)=\frac{1+\tau^2\Omega^2}{\tau}e^{-t/\tau}\cos(\Omega\tau) \tag{3.4}$$

was used to fit the correlation functions. This accounted for some small amplitude oscillatory behavior observed in the correlation functions. All calculations using nontrivial memory functions were compared to curve fits to the simple exponential form

$$C_{qq}(\mathbf{k},t)=Ae^{-k^2 D_T t} \ , \tag{3.5}$$

where A and D_T are adjustable parameters. The value of D_T calculated using the simple exponential form was generally comparable to the value obtained using the memory function.

Equation (3.2) can be easily solved via Laplace transforms. The result is

$$\tilde{C}_{qq}(\mathbf{k},z)=\frac{1}{-iz+\tilde{\phi}(z)D_T k^2}C_{qq}(\mathbf{k},0) \ , \tag{3.6}$$

where the tilde designates Laplace transforms. For the simple exponential relaxation function in Eq. (3.3), the inverse transform of Eq. (3.6) can be performed analytically [15]; but for more complicated $\phi(t)$, finding an analytic form for the inverse transform of Eq. (3.6) rapidly becomes unwieldy.

The inverse of Eq. (3.6) can be obtained numerically by first converting $\tilde{C}_{qq}(\mathbf{k},z)$ to the Fourier transform of $C_{qq}(\mathbf{k},t)$. Since $C_{qq}(\mathbf{k},t)$ is symmetric, $C_{qq}(\mathbf{k},\omega)$ is real. A standard result then relates $\tilde{C}_{qq}(\mathbf{k},z)$ to $C_{qq}(\mathbf{k},\omega)$ [13]:

$$C_{qq}(\mathbf{k},\omega)=\lim_{\eta\to 0} 2\,\mathrm{Re}[\tilde{C}_{qq}(\mathbf{k},\omega+i\eta)] \ . \tag{3.7}$$

Analytic expressions for $\tilde{C}_{qq}(\mathbf{k},\omega)$ can be obtained for most of the simpler forms of $\phi(t)$. The limit on the right-hand side of Eq. (3.7) is usually straightforward, and η can be set equal to zero without worrying about any singularities in $\tilde{C}_{qq}(\mathbf{k},z)$. Once $C_{qq}(\mathbf{k},\omega)$ is calculated, $C_{qq}(\mathbf{k},t)$ can be found using standard Fourier techniques. Equation (3.7) can also be used to calculate the derivatives of $C_{qq}(\mathbf{k},t)$ with respect to any parameters in the memory function $\phi(t)$. This is useful for curve-fitting models for $C_{qq}(\mathbf{k},t)$ to data generated from simulations.

The curve fits were performed by minimizing the objective function [16]

$$\chi(\{\alpha\})=\sum_{i=1}^{i_{\max}}\frac{(C_{qq}(\mathbf{k},t_i)-C_{qq}(\mathbf{k},t_i;\{\alpha\}))^2}{\sigma_i^2} \ , \tag{3.8}$$

where the $C_{qq}(\mathbf{k},t_i)$ are the measured values of the correlation functions at the times t_i, and the $C_{qq}(\mathbf{k},t_i;\{\alpha\})$ are the corresponding values of the analytic form, which depend on the parameters $\{\alpha\}$. One of the parameters in $\{\alpha\}$ should always be D_T. The σ_i are the uncertainties associated with the measured $C_{qq}(\mathbf{k},t_i)$. The uncertainties σ_i are generally much harder to calculate than the average values $C_{qq}(\mathbf{k},t_i)$ and accurate values of σ_i would require considerably more computational effort. For curve fits, only the relative magnitudes of the σ_i are needed, so following Ref. [3] the approximation

$$\sigma_i^2 \sim t_i$$

is used. The proportionality constant is not needed since it does not change the location of the minimum. This form accounts for the increasing uncertainty in the $C_{qq}(\mathbf{k},t_i)$ at longer times.

For small enough values of k, the value of D_T obtained from the curve fits will be independent of k, but at larger values the thermal diffusivity may begin to exhibit some k dependence. Because both $C_{qq}(\mathbf{k},t)$ and the analytic forms represented by Eq. (3.6) are rigorously even functions of k, the small-k behavior must have the form

$$D_T(k)=D_T^\infty+ak^2+O(k^4) \ . \tag{3.9}$$

The $D_T(k)$ calculated from the $C_{qq}(\mathbf{k},t)$ can be fit to Eq. (3.9) and used to extrapolate $D_T(k)$ to the $k\to 0$ limit. This procedure is valid so long as k is small enough so that higher-order terms in k do not contribute to the behavior of $D_T(k)$.

IV. RESULTS

The results of simulations on the Lennard-Jones fluid, carbon dioxide, and water are reported. The simulations were all performed at constant energy using the velocity Verlet algorithm recast as a predictor corrector [11]. The molecular systems were treated as rigid molecules, and the internal constraints were maintained using a variant of the SHAKE algorithm [17,18]. The standard truncated potential

$$\phi(r)=4\epsilon\left[\left[\frac{\sigma}{r}\right]^{12}-\left[\frac{\sigma}{r}\right]^{6}\right]+\phi_0$$

was used for the Lennard-Jones fluid, where ϵ is the well depth and σ is the hard-sphere radius. The constant ϕ_0 is chosen so that the potential vanishes at the cutoff distance r_c. The potentials for carbon dioxide and water both consist of pairwise additive terms $\phi_{ij}(r_{ij})$ which are formed from Lennard-Jones functions and Coulomb interactions. The $\phi_{ij}(r_{ij})$ were truncated by adding terms of the form

$$a_{ij}+b_{ij}(r_{ij}-r_c)\ ,$$

and choosing a_{ij} and b_{ij} so that both $\phi_{ij}(r_{ij})$ and its derivative with respect to r_{ij} vanished at the cutoff distance. For the Lennard-Jones fluid, the cutoff was set at $r_c=2.5\sigma$; for carbon dioxide and water, the cutoff was set at $r_c=9.5$ Å.

The $C_{qq}(\mathbf{k},t)$ were calculated from constant energy simulations. The energy was adjusted until the average temperature matched the target temperature. For most of the individual simulations, the average temperature was within 2 K of the target temperature (the only exception was one of the 500-molecule simulations of carbon dioxide). The time step for the water and carbon dioxide simulations was 2.5 fs while for the Lennard-Jones fluid it was 0.0047 in reduced time units, where $t^*=t/\sqrt{m\sigma^2/\epsilon}$ for a particle of mass m [19].

Several separate simulations were run for each system. Within each simulation, the individual $C_{qq}(\mathbf{k},t)$ were calculated using multiple time origins separated by 0.01 ps (0.0235 in reduced units for the Lennard-Jones fluid). For each simulation, the $C_{qq}(\mathbf{k},t)$ for all independent wave vectors corresponding to a given set of indices were calculated and the average taken to get a single correlation function. For the indices (1,0,0) there are six separate contributions, for (1,1,0) there are twelve contributions, and for (1,1,1) there are eight. These individual contributions to the $C_{qq}(\mathbf{k},t)$ were combined at the end of each simulation to give an average $C_{qq}(\mathbf{k},t)$ for the simulation. For each fluid, simulations on two different size systems were performed. These provided the TCAF's for a total of six different values of k for each fluid.

A. Lennard-Jones fluid

For comparison with other workers, simulations of the Lennard-Jones fluid were performed at the state point $\rho^*=0.8442$, $T^*=0.722$. The asterisk indicates the reduced units $\rho^*=\rho\sigma^3$ and $T^*=k_BT/\epsilon$. The thermal conductivity has been calculated at this state point using both the Green-Kubo relation and NEMD techniques. The present work included four simulations on a system containing 1372 particles and four simulations on a system containing 864 particles. Each simulation was 50 000 steps long. The values of $D_T(k)$ were calculated using the curve-fitting procedure described above. Fits of $C_{qq}(\mathbf{k},t)$ were done using both the simple exponential decay represented by Eq. (3.5) and the more complicated memory function form of Eq. (3.6) using the memory kernel given by Eq. (3.3). In all cases, the values of D_T obtained from the two procedures agreed to within 1.5%. The three $C_{qq}(\mathbf{k},t)$ from a single 1372-particle simulation are plotted in Fig. 1, along with the fits to the memory function form of the diffusion equation.

The curve fits match the data quite closely for all three correlation functions. The correlation functions themselves are relatively simple. After an initial relaxation period of $t^*\sim0.1$, they settle down to a simple monotonic decay, consistent with the exponential form in Eq. (2.18).

The calculated values of D_T^* are plotted as a function of k^* in Fig. 2. Also included in Fig. 2 is the fit to the parabolic form represented by Eq. (3.9). Within the uncertainty in the data, the points from different size simulations appear to lie on the same curve. This indicates that the $C_{qq}(\mathbf{k},t)$ do not depend significantly on the size of the system used to calculate them. The parameters from the fit are $D_T^{\infty *}=1.46\pm0.07$ and $a^*=-0.273\pm0.091$. The uncertainties are obtained using standard regression analysis [20] and represent 95% confidence intervals. Although the data in Fig. 2 are fairly noisy, it suggests that there might be a change in the behavior of $D_T^*(k^*)$ in the vicinity of $k^*\sim0.8$. At higher values of k^*, the function $D_T^*(k^*)$ appears to flatten out slightly. As a check, a second fit to the parabola (3.9) was done using only the points for $k^*<0.8$. The parameters change only slightly to $D_T^{\infty *}=1.52\pm0.15$ and $a^*=-0.404\pm0.160$. Within the uncertainties, the differences in the two fits are insignificant.

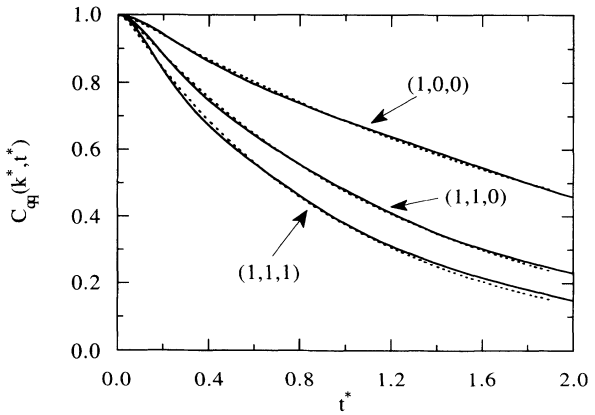

FIG. 1. $C_{qq}(\mathbf{k},t)$ for the Lennard-Jones fluid are plotted for the (1,0,0), (1,1,0), and (1,1,1) wave vectors. Time is in reduced units. The solid lines are calculated from a single simulation of 1372 particles; the dotted lines are the curve fits to the memory function form (3.6) using the simple exponential memory kernel (3.3).

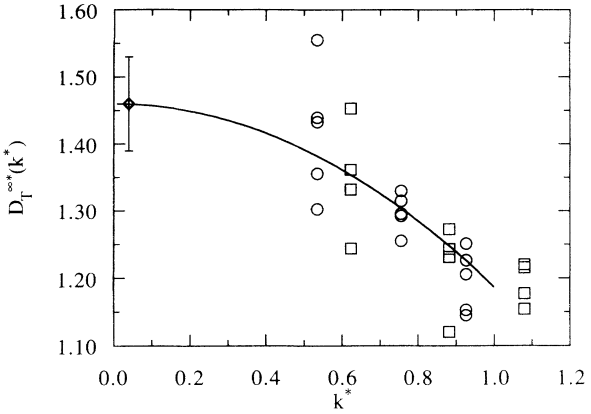

FIG. 2. Thermal diffusivity as a function of wave vector for the Lennard-Jones fluid. Both thermal diffusivity and wave vector are in reduced units. The circles are calculated from the 1372-particle simulations; the squares are calculated from the 864-particle simulations. The solid line is a least-squares fit to Eq. (3.9). The value of $D_T^{\infty *}$, along with its uncertainty, is given by the diamond symbol near the left edge of the plot.

To compare the value of D_T^* with the thermal conductivity calculated by other authors, a series of eight simulations were run on a 500-particle system using the constant-pressure constant-temperature algorithm of Andersen and Nosé [21,22]. The simulations were run at the reduced pressure $p_{ex}^* = p_{ex}\sigma^3/\epsilon = 0.896$ and the reduced temperature $T^* = 0.722$. Each simulation was 50 000 steps long. The mean-square fluctuations in the enthalpy

$$H = E + pV$$

were calculated and the constant-pressure specific heat was obtained from the relation [11]

$$c_p = \frac{\langle \delta H^2 \rangle_{N_p T}}{N k_B T^2} .$$

The brackets $\langle\ \rangle_{N_p T}$ indicate averages in the isothermal-isobaric ensemble. The externally applied pressure is used for the pressure p appearing in H and not the instantaneous pressure. The average density for these simulations was 0.8438 ± 0.0002, which is close to the density of $\rho^* = 0.8442$ used in the constant-energy simulations. The value of the constant-pressure specific heat from these simulations was $c_p/k_B = 5.02 \pm 0.74$. From Eq. (1.1), the thermal conductivity corresponding to $D_T^{\infty *} = 1.46$ is $\kappa^* = \kappa(m\sigma^3/\epsilon k_B) = 6.18 \pm 1.22$. This is slightly lower than the value of 6.78 ± 0.17 obtained by Paolini, Ciccotti, and Massabrio using an NEMD calculation [7], but the two values agree within the uncertainties. The value of κ^* corresponding to $D_T^{\infty *} = 1.52$ is $\kappa^* = 6.44 \pm 1.59$. The overall agreement of the plane wave and NEMD calculations is fairly good, but the plane-wave method appears to have much higher uncertainties associated with it.

B. Carbon dioxide

The simulations of carbon dioxide were done using a modified version [23] of the Murthy-Singer-McDonald (MSM) potential [24]. A series of four simulations on a 500-molecule system and four simulations on a 256-molecule system were performed. For both system sizes, the individual simulations were 50.0 ps long. The temperature was set at 290 K and the density was set at the liquid saturation density of 0.798 g/cm^3. Previous simulations of this potential, using both Ewald sums and truncations for the long-range forces, have shown that this model accurately reproduces a large number of the experimental properties of carbon dioxide [3,18,23,24].

The $C_{qq}(\mathbf{k},t)$ from one of the 256-molecule simulations, along with the curve fits to the exponential decay (3.5), are shown in Fig. 3. Attempts to fit these curves to the more general memory function form using the simple exponential memory kernel (3.3) were unsuccessful in about half the cases. When fits using the memory function form were obtained, the value of τ in the kernel (3.3) was always less than 0.1 ps and in many cases was on the order of ~ 0.01–0.02 ps. This is comparable to the sampling frequency, so τ is probably not well determined by the data. However, in all cases where fits were obtained using both the memory function form and the simple exponential decay, the difference in the values of D_T obtained by the two methods was less than 0.2%.

The values of D_T are plotted as a function of k in Fig. 4. Although the scatter in the points is too great to make a meaningful determination, there are no obvious indications that the $D_T(k)$ from different size simulations lie on different curves. The fit to the quadratic form (3.9) is also shown. The parameters derived from the fit are $D_T^{\infty} = (4.25 \pm 0.88) \times 10^{-4}$ cm^2/s and $a = (6.6 \pm 10.1) \times 10^{-4}$ cm^2 Å^2/s. The value of D_T^{∞} is about 45% higher than the experimental number of 2.92×10^{-4} cm^2/s [25,26], although the uncertainties in D_T^{∞} are large. The slow relaxation times, on the order of 4–7 ps for the smaller values of k, may contribute to the noise. Because

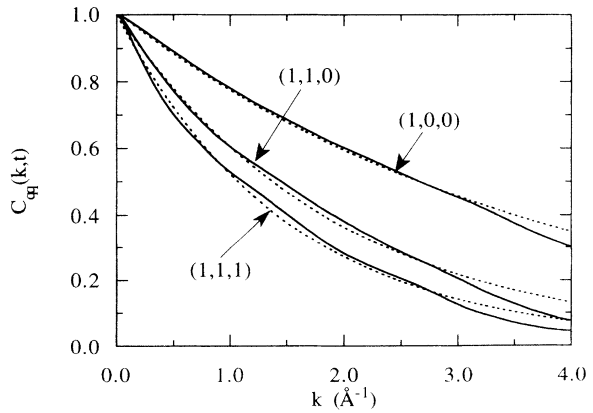

FIG. 3. $C_{qq}(\mathbf{k},t)$ for the MSM model of carbon dioxide are plotted for the (1,0,0), (1,1,0), and (1,1,1) wave vectors. The solid lines are calculated from a single simulation of 256 molecules; the dotted lines are the curve fits to the exponential decay (3.5).

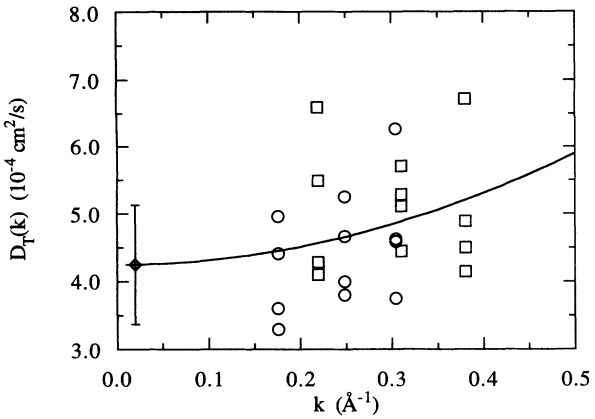

FIG. 4. Thermal diffusivity as a function of wave vector for the MSM model of carbon dioxide. The circles are calculated from the 500-molecule simulations; the squares are calculated from the 256-molecule simulations. The solid line is the least-squares fit to Eq. (3.9). The value of D_T^∞, along with its uncertainty, is given by the diamond symbol near the left edge of the plot.

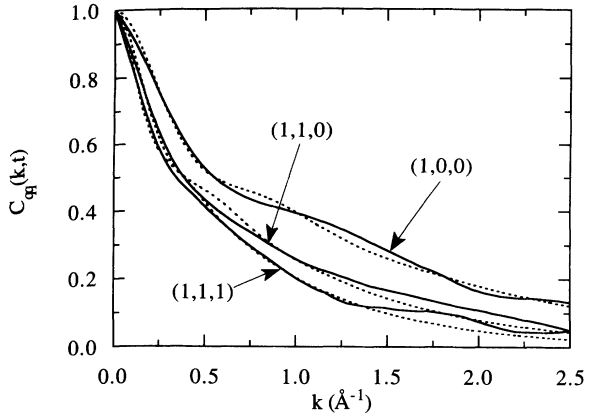

FIG. 5. $C_{qq}(\mathbf{k},t)$ for the TIP4P model of water are plotted for the (1,0,0), (1,1,0), and (1,1,1) wave vectors. The solid lines are calculated from a single simulation of 500 molecules; the dotted lines are the curve fits to the memory function form (3.6) using the oscillating memory kernel (3.4).

the relaxation times are so long, there are relatively few uncorrelated intervals in each simulation, and the number of independent events contributing to each $C_{qq}(\mathbf{k},t)$ is small.

The positive value for the coefficient a is unusual, given that the value for a for both the Lennard-Jones fluid and water is negative. The uncertainty in a is large enough so that a small negative value for a is a reasonable possibility. Even for the value of a obtained in the fit, the data suggests that the values of D_T are only weakly dependent on k for $k<0.4$ Å^{-1}. A straight average of the data gives a value of $D_T=(4.77\pm0.40)\times10^{-4}$ cm^2/s, which is not significantly different from the value obtained by fitting $D_T(k)$ to the parabola (3.9).

C. TIP4P water

The simulations on water were done using the TIP4P model of Jorgensen *et al.* [27]. As with carbon dioxide, a series of four simulations on a 500-molecule system and four simulations on a 256-molecule system were performed. Each simulation was 50.0 ps long. The temperature was set at 298 K and the density was set at the one-atmosphere density of 0.997 g/cm^3.

The results for water are somewhat curious. The $C_{qq}(\mathbf{k},t)$ from one of the 500-molecule simulations are shown in Fig. 5, along with the curve fits to the memory function form (3.6) using the oscillatory memory kernel (3.4). Attempts to use the simple exponential decay (3.5) for the memory kernel were consistently unsuccessful. The simulation curves all appear to show a weak oscillation on top of the slow decay of the correlation function, or at least a break in the decay in the neighborhood of 0.5 ps. The overall quality of the curve fits is quite poor; the memory function seems to oscillate more than the data at short times and less at longer times [the second break in the (1,0,0) curve near 2 ps is consistently reproducible from one simulation to the next]. There is also a noticeable difference in the values of $D_T(k)$ obtained using the memory function form compared to the simple exponential decay. The values of $D_T(k)$ obtained from fitting the exponential are 5–10% higher than the corresponding values obtained using the memory function form.

The D_T obtained using the memory function form for $C_{qq}(\mathbf{k},t)$ are plotted as a function of k in Fig. 6, along with the fit to the parabolic form (3.9). Again, the $D_T(k)$ for the different system sizes appear to lie on the same curve. The parameters derived from the curve fit are $D_T^\infty=(1.51\pm0.18)\times10^{-3}$ cm^3/s and $a=(-3.14\pm0.95)\times10^{-3}$ cm^2 Å^2/s. Like the Lennard-Jones results, the data in Fig. 6 appear to flatten out slightly at larger values of k. Fitting only the points for $k<0.4$ Å^{-1} gives the parameters $D_T^\infty=(1.91\pm0.50)\times10^{-3}$ cm^2/s and $a=(-7.03\pm4.88)\times10^{-3}$ cm^2 Å^2/s. The difference in D_T^∞ from the two fits falls within the uncertainties. How-

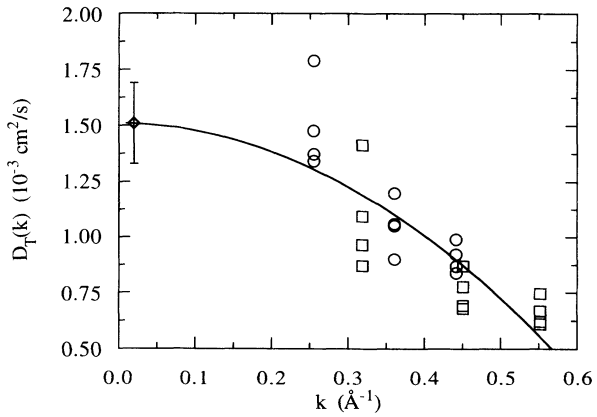

FIG. 6. Thermal diffusivity as a function of wave vector for the TIP4P model of water. The circles are calculated from the 500-molecule simulations; the squares are calculated from the 256-molecule simulations. The solid line is the least-squares fit to Eq. (3.9). The value of D_T^∞, along with its uncertainty, is given by the diamond symbol near the left edge of the plot.

ever, the difference does lie near the edge of the uncertainty and suggests that there may be a crossover in the behavior of $D_T(k)$ near $k \sim 0.4$ Å^{-1}. The experimental value for the thermal diffusivity of water is 1.46×10^{-3} cm^3/s [28]. This compares very well with the fit to the full data set, but is significantly lower than the number obtained when only the points for $k < 0.4$ Å^{-1} are used. The overall conclusion is that the thermal diffusivity for the TIP4P model of water is probably slightly higher than the experimental number for water.

If the $D_T(k)$ calculated by fitting the $C_{qq}(\mathbf{k},t)$ to the simple exponential decay (3.5) are fit to the parabola (3.9), the results parallel those obtained for the data shown in Fig. 6. A fit to all the data points gives the parameters $D_T^{\infty} = (1.63 \pm 0.18) \times 10^{-3}$ cm^2/s and $a = (-3.40 \pm 0.96) \times 10^{-3}$ cm^2 Å^2/s, while the fit to only the points for $k < 0.4$ Å^{-1} gives $D_T^{\infty} = (2.06 \pm 0.48) \times 10^{-3}$ cm^2/s and $a = (-7.69 \pm 4.66) \times 10^{-3}$ cm^2 Å^2/s. It is encouraging that the numbers are so close for both sets of curve fits, even for a case where neither model for $C_{qq}(\mathbf{k},t)$ is particularly good.

The slight oscillatory behavior in the $C_{qq}(\mathbf{k},t)$ is probably not due to any microscopic relaxation processes. It more likely results from the second term in Eq. (2.16), which can contribute to the behavior of $C_{qq}(\mathbf{k},t)$ for finite values of k. The values of Ω in the memory kernel (3.4) are plotted as a function of k in Fig. 7. The plot suggests that $\Omega(k)$ vanishes as $k \to 0$. If Ω were determined by some intrinsic microscopic process, then Ω should depend only weakly on k, and have a finite value at $k = 0$. On the other hand, if the oscillation is due to the second term in (2.16), the Ω would be expected to depend on k in the manner suggested by Fig. 7. The frequency of pressure oscillations vanishes linearly as the wavelength of the oscillation goes to infinity, which resembles the behavior in Fig. 7. The behavior of Ω, combined with the nonexponential form of the $C_{qq}(\mathbf{k},t)$, suggests that water is still fairly far from the small-k limit for the 500-molecule system. Because of the connection between $C_{qq}(\mathbf{k},t)$ and the Green-Kubo formula for κ, there may be a noticeable size dependence for Green-Kubo values of κ calculated from simulations in this size range.

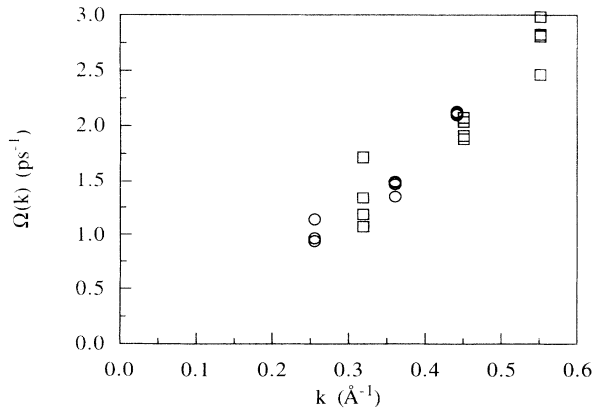

FIG. 7. The value of Ω in the memory kernel (3.4) as a function of wave vector for the TIP4P model of water. The circles are calculated from the 500-molecule simulations; the squares are calculated from the 256-molecule simulations.

V. CONCLUSIONS

The calculation of the thermal diffusivity from fluctuations in the heat energy density $q(\mathbf{r},t)$ represents a viable method of estimating the thermal diffusivity from equilibrium molecular-dynamics simulations. Whether the method can be used to obtain high accuracy results remains to be seen. For the Lennard-Jones fluid, the thermal diffusivity calculated from fluctuations in $q(\mathbf{r},t)$ is in agreement with the thermal conductivity calculated using NEMD techniques. The fluctuation method is easy to implement and does not add significantly to the cost of the simulation. The statistics for this method appear to be poorer than for the Green-Kubo and NEMD methods, and the analysis of the $C_{qq}(\mathbf{k},t)$ is more complicated than integrating the Green-Kubo integrand.

The determination of where the small-k region begins remains the most subjective aspect of calculating the D_T from the $C_{qq}(\mathbf{k},t)$. For large values of k, the behavior of $C_{qq}(\mathbf{k},t)$ may deviate from the simple exponential form—not only because of nonhydrodynamic behavior at short wavelengths, but also because of *hydrodynamic* coupling between the heat energy density $q(\mathbf{r},t)$ and the pressure field $p(\mathbf{r},t)$ at finite k. The hydrodynamic couplings could, in principle, be incorporated into the calculation by simultaneously solving the linearized hydrodynamic equations for $q(\mathbf{r},t)$,$p(\mathbf{r},t)$, and the longitudinal component of the velocity field [15].

Unlike the Green-Kubo integral and NEMD simulations, the $C_{qq}(\mathbf{k},t)$ lead directly to the thermal diffusivity instead of the thermal conductivity. These two transport coefficients can be related via Eq. (1.1), but this requires the calculation of the constant-pressure specific heat. The calculations of c_p for the Lennard-Jones fluid indicate that determining the constant-pressure specific heat to high accuracy is likely to be a computationally intensive task. If the thermal diffusivity is the desired quantity, the direct approach using the $C_{qq}(\mathbf{k},t)$ is probably more efficient than the indirect calculation using Eq. (1.1).

Several authors have noted that the Green-Kubo integrand for the thermal conductivity decays rapidly in zero and does not exhibit the long-time tail seen in the Green-Kubo integrand used to calculate the shear viscosity [1,10]. For the Lennard-Jones fluid and carbon dioxide, the $C_{qq}(\mathbf{k},t)$ rapidly reach behavior that is compatible with the exponential decay predicted by the hydrodynamic theory for small values of k. Even for water, the $C_{qq}(\mathbf{k},t)$ show only small deviations from the expected behavior.

For the shear viscosity, the correlation function analogous to $C_{qq}(\mathbf{k},t)$ is the transverse current autocorrelation function. Like the $C_{qq}(\mathbf{k},t)$, the TCAF's decay exponentially in the small-k, long-time limit. However, the TCAF's for the Lennard-Jones fluid and water are significantly different from an exponential decay in the range of system sizes investigated here. The large-k TCAF's for the Lennard-Jones fluid ($k^* > 0.8$) and all the TCAF's for water exhibit damped oscillatory behavior. The slower approach to hydrodynamic behavior for the TCAF's may be related to the existence

of the long-time tail in the Green-kubo integrand.

Finally, it is worth noting that the values of D_T obtained from the simulations of carbon dioxide and water are within at least a factor of 2 of the experimental values, and are more likely within 50% of experiment. This agreement suggests that it should be possible to obtain qualitative information about thermal diffusion in molecular liquids from classical simulations. Whether it is possible to obtain quantitative agreement for molecular liquids is a more complicated question. As Eq. (1.1) indicates, the thermal conductivity and the thermal diffusivity are related by a factor of the constant-pressure specific heat. For molecular liquids, the constant-volume specific heat c_v is known to have substantial quantum corrections [29], and this would be expected of c_p as well ($c_p \sim c_v$ for most molecular liquids). Thus, either the thermal conductivity or the thermal diffusivity is likely to have a large quantum correction, which would limit the absolute accuracy that can be achieved with a classical model.

ACKNOWLEDGMENTS

This work was supported by Conservation and Renewable Energy, Office of Industrial Technologies, Advanced Industrial Concepts Program, U.S. Department of Energy, under Contract No. DE-AC06-76RLO 1830. Pacific Northwest Laboratory is operated for the U.S. Department of Energy by Battelle Memorial Institute.

[1] C. Hoheisel and R. Vogelsang, Comput. Phys. Rep. **8**, 1 (1988).
[2] M. Schoen and C. Hoheisel, Mol. Phys. **65**, 653 (1985).
[3] B. J. Palmer, Phys. Rev. E (to be published).
[4] L. Landau and E. M. Lifshitz, *Fluid Mechanics* (Pergamon, Oxford, 1959).
[5] D. J. Evans, Phys. Lett. **91A**, 457 (1982).
[6] C. Massabrio and G. Ciccotti, Phys. Rev. A **30**, 3191 (1984).
[7] G. V. Paolini, G. Ciccotti, and C. Massabrio, Phys. Rev. A **34**, 1335 (1986).
[8] R. Vogelsang, C. Hoheisel, and G. Ciccotti, J. Chem. Phys. **86**, 6371 (1987).
[9] C. Hoheisel, J. Chem. Phys. **89**, 3195 (1988).
[10] H. Luo and C. Hoheisel, J. Chem. Phys. **96**, 3173 (1992).
[11] M. P. Allen and D. J. Tildesley, *Computer Simulation of Liquids* (Clarendon, Oxford, 1987).
[12] L. P. Kadanoff and P. C. Martin, Ann. Phys. **24**, 419 (1963).
[13] D. Forster, *Hydrodynamics, Fluctuations, Broken Symmetry and Correlation Functions* (Benjamin/Cummings, Reading, MA, 1975).
[14] J.-P. Hansen and I. R. McDonald, *Theory of Simple Liquids,* 2nd ed. (Academic, London, 1986).
[15] J. P. Boon and S. Yip, *Molecular Hydrodynamics* (Dover, New York, 1991).
[16] W. H. Press, B. P. Flannery, S. A. Teukolsky, and W. T. Vetterling, *Numerical Recipes* (Cambridge University Press, Cambridge, 1988).
[17] B. J. Palmer, J. Comput. Phys. **104**, 470 (1993).
[18] B. J. Palmer and B. C. Garrett, J. Chem. Phys. **98**, 4047 (1993).
[19] There are two definitions of reduced time in the literature; these differ by a factor of $\sqrt{48}$.
[20] J. Neter, W. Wasserman, and M. H. Kutner, *Applied Linear Statistical Models* (Irwin, Homewood, IL, 1985).
[21] H. C. Andersen, J. Chem. Phys. **72**, 2384 (1980).
[22] S. Nosé, J. Chem. Phys. **81**, 511 (1984).
[23] L. C. Geiger, B. Ladanyi, and M. E. Chapin, J. Chem. Phys. **93**, 4533 (1990).
[24] C. S. Murthy, K. Singer, and I. R. McDonald, Mol. Phys. **44**, 135 (1981).
[25] *Thermophysical Properties of Matter,* edited by Y. S. Touloukian, P. E. Liley, and S. C. Saxena (IFI/Plenum, New York, 1970), Vol. 3. The thermal diffusivity for carbon dioxide was derived from the thermal conductivity and the constant pressure specific heat.
[26] *Thermophysical Properties of Matter,* edited by Y. S. Touloukian and T. Makita (IFI/Plenum, New York, 1970), Vol. 6.
[27] W. L. Jorgensen, J. Chandrasekhar, J. D. Madura, R. W. Impey, and M. L. Klein, J. Chem. Phys. **79**, 926 (1983).
[28] *Thermophysical Properties of Matter,* edited by Y. S. Touloukian, R. W. Powell, C. Y. Ho, and M. C. Nicolaou (IFI/Plenum, New York, 1973), Vol. 10.
[29] P. H. Berens, D. H. J. MacKay, G. M. White, and K. R. Wilson, J. Chem. Phys. **79**, 2375 (1983).